We are IntechOpen, the world's leading publisher of Open Access books Built by scientists, for scientists

6,900
Open access books available

186,000
International authors and editors

200M
Downloads

154
Countries delivered to

Our authors are among the

TOP 1%
most cited scientists

12.2%
Contributors from top 500 universities

CLARIVATE ANALYTICS
BOOK CITATION INDEX
INDEXED

WEB OF SCIENCE™

Selection of our books indexed in the Book Citation Index
in Web of Science™ Core Collection (BKCI)

Interested in publishing with us?
Contact book.department@intechopen.com

Numbers displayed above are based on latest data collected.
For more information visit www.intechopen.com

New Approaches to Preparation of SnO$_2$-Based Varistors — Chemical Synthesis, Dopants, and Microwave Sintering

Glauco M.M.M. Lustosa, Natalia Jacomaci, João P.C. Costa,
Gisane Gasparotto, Leinig A. Perazolli and Maria A. Zaghete

Additional information is available at the end of the chapter

Abstract

Tin oxides have applications such as sensors, solar cells, transistors, and varistors, which are being studied to replace ZnO varistors due to similar electrical properties, simpler microstructure, no formation of secondary phases, and lower concentration of agent modifiers to promote the varistor characteristics and densification. Varistors are ceramic with a high concentration of structural and electronics defects. The type and the amount of defects are related with agent modifiers and processing steps employed. The study in materials processing aims to improve the ceramics properties. Chemical synthesis ensures the homogeneous distribution of dopants used to promote electrical and structural properties. Microwave sintering appears as processing to optimize time and sintering temperature. Varistor application is linked to its breakdown voltage, which should be larger than the operating voltage. In an operating range of 1 kV to 1 MV, the varistors are used in electricity transmission networks. In a range of 24–1000 V, the application occurs in electronics and appliances and in a range smaller than 24 V, as protective of automotive electronics and computers. This chapter aims to provide information on new processing steps for the production of SnO$_2$ varistors and to show the possibility to get electrical properties with non-ohmic characteristic for technological applications.

Keywords: Tin dioxide varistor, chemical synthesis, microwave sintering, dopants, low voltage

1. Introduction

1.1. Varistors

Varistor is an electrical device based on semiconductor materials used for protection against voltage spikes in the electric network, against overvoltage in electronic circuits of low voltage and electrical power systems [1,2].

Due to the high energy absorption, the ceramic varistors become many helpful in protecting electrical circuits, and their electrical properties are highly dependent on their microstructure. The development of devices ever more technological and brings the need for electrical protection due to the sensitivity equipment. The use of varistors as voltage protectors in electronic equipment is very simple: the varistor is directly connected in parallel to the power line of equipment, and in case of an increase in the electrical current on energy network, the varistor rapidly increases the conductivity, allowing the current flow toward the ground. For electrical appliances operating with few voltages, the varistors ceramics are called low-voltage varistors [1–3].

The first varistor ceramics were developed in 1930. They were constituted from compact silicon carbide (SiC) partially sintered and were designed by the System Bell Labs to replace selenium rectifiers that were used in the protection of telephone systems [4]. Over time, the processing of varistors has undergone successive improvements, and in 1968, Matsuoka [3] developed varistors based on zinc oxide with manganese and cobalt as a dopant to improve the electrical properties. One of the disadvantages of using ZnO-based varistors are the large amount of dopant added to ceramic matrix for its electric modification and consequently to its high chemical instability that leads to degradation of the varistor. Castro et al. [5] reported that the trapping of electrons, ion migration and oxygen adsorption are included as ZnO varistor degradation mechanisms. The exposure of ZnO varistors to high temperatures and oxidizing atmospheres leads to excess interstitial ions $D_{Zn}^{\cdot}$ and $D_{Zn}^{\cdot\cdot}$ that migrate through the depletion layer and chemically interact with species that are in the grain boundary, causing decrease and enlargement of the potential barrier, and facilitate the electronic conduction, destroying its varistor property [5,6].

The SnO$_2$-based varistors were introduced by Pianaro et al. [7] as an alternative to the ZnO varistors commercial, presenting nonlinear electrical characteristics similar to ZnO varistors. The SnO$_2$-based system shows more advantages, for example, their simpler microstructure and no formation of secondary phases require a lower concentration of agents modifiers to promote the varistor characteristics and densification and higher chemical and thermal resistances. The use of M^{2+} ion as dopant improved significantly the densification of the varistor, the addition of M^{5+} ion promoted electrical conductivity, and the M^{3+} ion influenced on nonlinearity coefficient.

1.2. Electrical properties

The electrical properties of varistor ceramics are governed by potential barriers located in the grain boundaries. Potential barriers were formed by the addition of dopants elements to

generate defects on crystal network, which segregate to the grain boundary region by diffusion during sintering. The presence of these barriers promotes the large-capacity power absorption and its flow when subjected to electrical overvoltage [4,8].

In denominated "smart ceramics," the ceramic varistor acts as variable resistors, with resistive behavior at low voltages and conductive behavior starting from a specific voltage value, known as the breakdown voltage (V_R) or breakdown electric field (E_R) [9,10].

These electrical responses featuring the varistor ceramics as main elements in the manufacture of devices for electrical protection equipment subjected to both low and medium voltages apply directly as of the electro-electronics components (telephony system, computers, medical devices, automotive electronics, industrial automation systems, alarms, transformers, etc.) and for the high voltages used as part of lightning protection devices installed in the terminals of the power substations [11].

The varistor characteristic associated to quality is the nonlinear coefficient (α). The higher their value, the greater the varistor efficiency. This coefficient can be obtained through empirical relationships current × voltage (Eq. 1) or current density versus electric field (Eq. 2) and expresses how much the material deviates from ohmic response when required, and it can be explained by a graphic representation (Figure 1) with distinct regions [12–15].

$$I = CV^{\alpha} \tag{1}$$

$$J = CE^{\alpha} \tag{2}$$

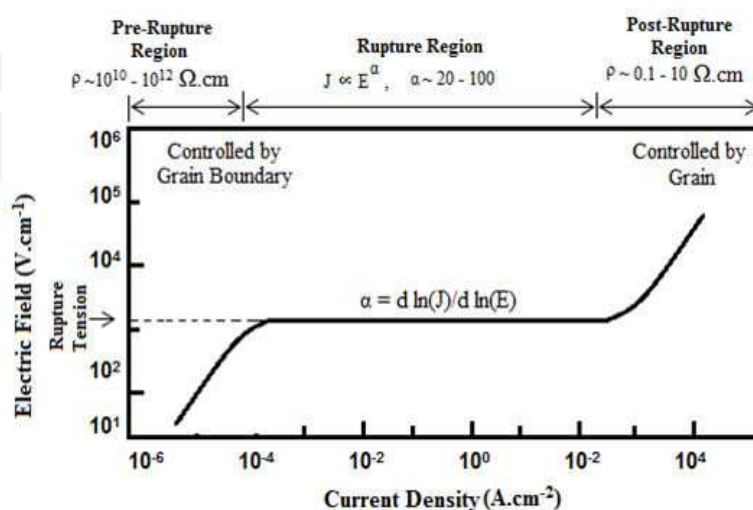where C is a constant related to the microstructure.

Figure 1. Electric field (E) versus current density (J) curves of a varistor [16].

The pre rupture region is also named as linear region and has an ohmic behavior when the material is under operation normal tension. The varistor acts as a resistor in this case with a small amount of current (known as leakage current) passing through the material due to the action of the potential barrier formed at grain boundary and preventing the electronic conduction between the grains. The conductivity in this region is of thermionic emission type, i.e., the electrical conduction is strongly dependent of temperature, thus being possible to retrieve information about the resistivity of the material [8,16,17].

The rupture region showed nonlinear behavior, i.e., non-ohmic behavior between the applied voltage and the current that the material is submitted. The conductivity of the material increases with a small variation in the applied voltage, indicating the varistor efficiency that starts to act as a conductor from a specific breakdown electric field (E_R). Recombination of electron-hole pair at grain boundary interfaces, thermionic emission, and electron tunneling are suggested as electric conduction mechanisms of this region [8,16].

In the post rupture region, the ohmic behavior between the current and the applied voltage is observed once again and is characterized by high current density. The electric conduction in this region is controlled by the impedance of the grains [2,8].

The V_R value provides the varistor voltage application, and it is a function of a grain size of sintered material. If the composition is fixed, the microstructure becomes strongly dependent on the processing conditions [12,15].

The varistor efficiency determined by the breakdown region can be evaluated by the α nonlinear coefficient of the curve in Figure 1, which is used in Eq. 6, derived from Eq. 3, which allows the calculation of the value of α by the field data electric (E) and current density (J) [18,19]:

$$\alpha = (logJ_2 - logJ_1) / (logE_2 - logE_1) \qquad (3)$$

The electric field and the current density are obtained from the measurements of the electric current (I) generated when the sample is submitted to a potential difference (V), according to Eqs. 4 and 5 [18,19]:

$$E = V/d \qquad (4)$$

$$J = I/A \qquad (5)$$

d is the thickness of the sample and A is the electrode area deposited on the film surface. For α calculation, the interval of 1 and 10 mA/cm^2 of current density was used, i.e., $J_1 = 1$ and $J_2 = 10$ [18,19]:

$$\alpha = (logE_2 - logE_1)^{-1} \qquad (6)$$

1.3. Mechanisms for electrical conduction

The potential barrier is the determining factor on the electrical properties of varistors. Several models have been proposed to better understand the potential barrier formed in the grain boundary region [20,21].

Gupta et al. [22] proposed the first potential barrier model for ZnO-based varistor of the Schottky-type with an intergranular layer acting as insulator between the grains. In this model, negative charge densities (formed by Zn vacancies) were trapped between the grain boundary being balanced by two depletion layers that are positively charged. Leite et al. [23] proposed the accumulation of oxygen species adsorbed as new origin of negative defects [22,23].

Based on the ZnO potential barriers model, Bueno et al. [14] suggested a modification for formation of potential barrier in SnO$_2$ varistors systems, whereas the sides of the barrier are in contact since there is no precipitated phase in the grain boundary, as observed Figure 2. In this model, the oxygen adsorbed species in the grain boundary region generate the negative charges defects, counterbalanced by the positive defects in the depletion layer. Pianaro et al. [1] proposed a potential barrier model, which has a large presence of negative charges on the SnO$_2$ surface generated by tin vacancies ($V_{sn}^{''}$), adsorbed oxygen atoms and substitutional cobalt ions ($Co_{Sn}^{''}$), and positive defects in the depletion layer formed by interstitial tin ($Sn^{\bullet\bullet\bullet\bullet}$, $Sn^{\bullet\bullet}$), oxygen vacancies ($V_O^{\bullet\bullet}$, $V_O^{\bullet}$), and niobium taking place of tin on the crystal lattice ($Nb_{Sn}^{\bullet}$) [1,14].
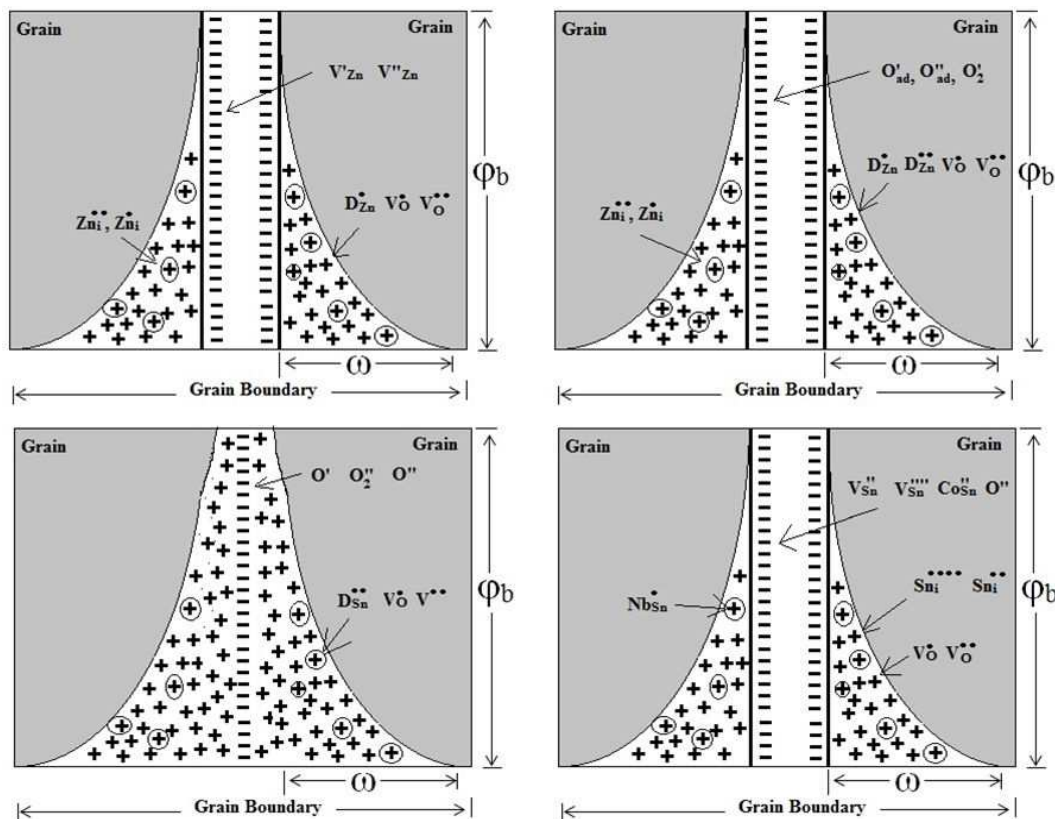

Figure 2. Potential barrier model to ZnO varistors proposed by Gutpa et al. [22] and Leite et al. [23] and to SnO$_2$ varistors base proposed by Bueno et al. [14] and Pianaro et al. [1].

1.3.1. Schottky type

In this model, the electrons are emitted and pass through the potential barriers particularly due to the action of temperature distorting the energy band diagram, near the interface. This distortion modifies the potential barrier favoring the thermal emission. The equation that describes this behavior is [24,25]

$$J_S = A^*.T_2.exp\left[-\frac{\phi_b - \beta E_{\frac{1}{2}}}{kT}\right]$$ (7)

where A^* is the Richardson constant, φ_b is the potential barrier height, E represents the electric field, T is the ambient temperature in Kelvin, and β is a constant related to the width of the potential barrier in accordance with the following equation [25]:

$$\beta = (n\omega)^{-1/2}$$ (8)

where n is the grain number per unit length and ω is the width of the barrier.

1.3.2. Poole–Frenkel type

The emission of the Poole–Frenkel type assumes the formation of coulombian centers in the grain–intergranular layer interface region. The relationship that describes this type of emission is on Equation 9, where the external electric field variations are more relevant than for issue of Schottky type [26]:

$$J_P = c.E.exp\left[-\frac{\phi_b - 2\beta E_{\frac{1}{2}}}{kT}\right]$$ (9)

where c is a constant of the material, T is the room temperature, E is the electric field, k is the Boltzmann constant, and φ_b is the height of the potential barrier. The thermionic emission cannot explain the high nonlinear coefficients observed in varistors. In the post rupture zone with the presence of high electric fields, the possibility that distortion of the energy levels and, therefore, the possibility that electrons pass through the potential barrier by tunneling must be considered [27].

2. Influence of synthesis methods on SnO_2 electrical properties

The processing by mixing oxides is widely used at the industrial scale for the production of varistor ceramics mainly due to its low cost, consisting basically of an initial powder mix and wet milling followed by drying, deagglomeration of powder, forming pellets/bulks, and

sintering. The varistor synthesis with large amounts of chemical additives and/or impurities resulting from the process can lead to non-densifying sintering mechanisms. This mean that impurities may accumulate on the material surface and increase the mass flow on the surface or forming more unstable compounds that can evaporate and condense on the surface, favoring grain growth without decreasing pore size. The advancement in ceramic materials process technology aims to find low-cost methods and the viability of the process on an industrial scale. Among the processes available in the literature for the production of ceramics, techniques can be cited as coprecipitation, sol-gel, dehydration by rapid cooling (freeze drying), combustion method, and polymeric precursor method known as the Pechini method [28–31].
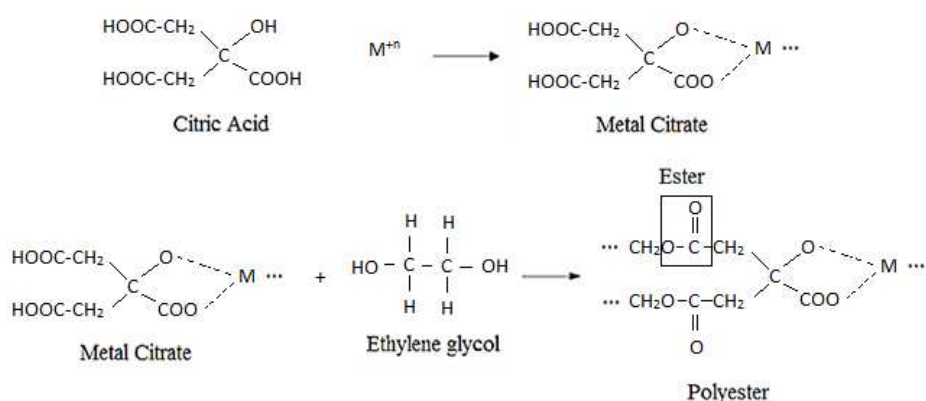

Figure 3. Schematic representation of reactions developed in the polymeric precursor method (Pechini method) [31].

The polymeric precursor method involves a complexation reaction of metal ions by an organic complexing agent as carboxylic acid. The metal ions are complexed into carboxylic sites forming a metal carboxylate, which is sequentially polymerized with ethylene glycol, as shown in Figure 3, citric acid is often used as the complexing agent. This process shows advantages such as low temperature of synthesis and high control of stoichiometry, and allows the obtention of powder with nanometric particles. The immobilization of metal ion in organic matrix reduces the segregation of the metal during the decomposition of the polymer at high temperatures, thus ensuring a homogeneous composition [31]. The ceramic powders are obtained by controlled calcination of the resin until total oxide formation.

Another method widely used for controlled synthesis of multifunctional ceramics is the sol-gel, that is used for the synthesis of a colloidal suspension where the dispersed phase is a solid and the dispersion medium is liquid, and is called sol. Therefore, there is the formation of a dual phase material: a solid body that is occupied by a solvent, i.e., moist gel. The initiator compounds, commonly called precursors, consist of a metal surrounded by many connections and typically are inorganic salts or organic compounds. The two precursors undergo two chemical reactions at sol preparation: hydrolysis and condensation, which resulted from the addition of an acid or base catalyst to form small solid particles or clusters in a liquid (aqueous solvent) [32,33]. The sol-gel method provides homogenous mixtures of cations on an atomic

scale and also allows the preparation of ceramic powders with high surface area and films or gels fibers, which have high technological importance. The method has advantages over other conventional methods such as high purity, resin calcination at low temperatures, and synthesis of oxides with defined and controlled properties [32–34].

Also, the controlled precipitation method (CPM) can be used to prepare precursor powders. In this case, the solution containing the cation of interest is added to another solution containing a precipitating agent that can be a base or anion (ammonia, urea, and oxalic acid). In this way, the final product precipitate is separated by filtration, washed, dried, and calcined to obtain the oxide. The precipitation process has a complex mechanism, which is dependent on the degree of saturation of the ion to be used. The process starts by formation of cluster from chemical species in the solution, known as nucleation process. Reaching the ion solubility limits the growth stage of formed centers and finally the formation of precipitates [35].

To check the influence of the chemical synthesis route the electrical properties of the SnO_2-based varistors, Mosquera et al. [36] carried out the synthesis of tin oxide by controlled precipitation and polymeric precursor (Pechini) methods that's offering the strict control of the chemical purity and the particle size of the raw material. The system $SnO_2.Co_3O_4.Nb_2O_5.TiO.Al_2O_3$, with 1 mol% Co_3O_4, 0.05 mol% Nb_2O_5, and 1 mol% TiO_2 and variations of 0.05 (named SCNT05A), 0.1 (named SCNT1A), and 0.2 mol% (named SCNT2A) of Al_2O_3 were prepared. Following synthesis, the materials were submitted to heat treatment at 600°C/1 h (controlled precipitation method, CPM) and 600°C/2 h (Pechini method, PCH) to eliminate organic matter and obtain the full formation of the oxide. The use of dopants in both methods resulted in no change in the SnO_2-crystal structure or formation of secondary phases due to have been added small amounts of dopants (Figure 4). The SEM micrographs indicated the influence of the addition of the aluminum grain growth control. The Pechini method showed smaller grains and more porous samples.
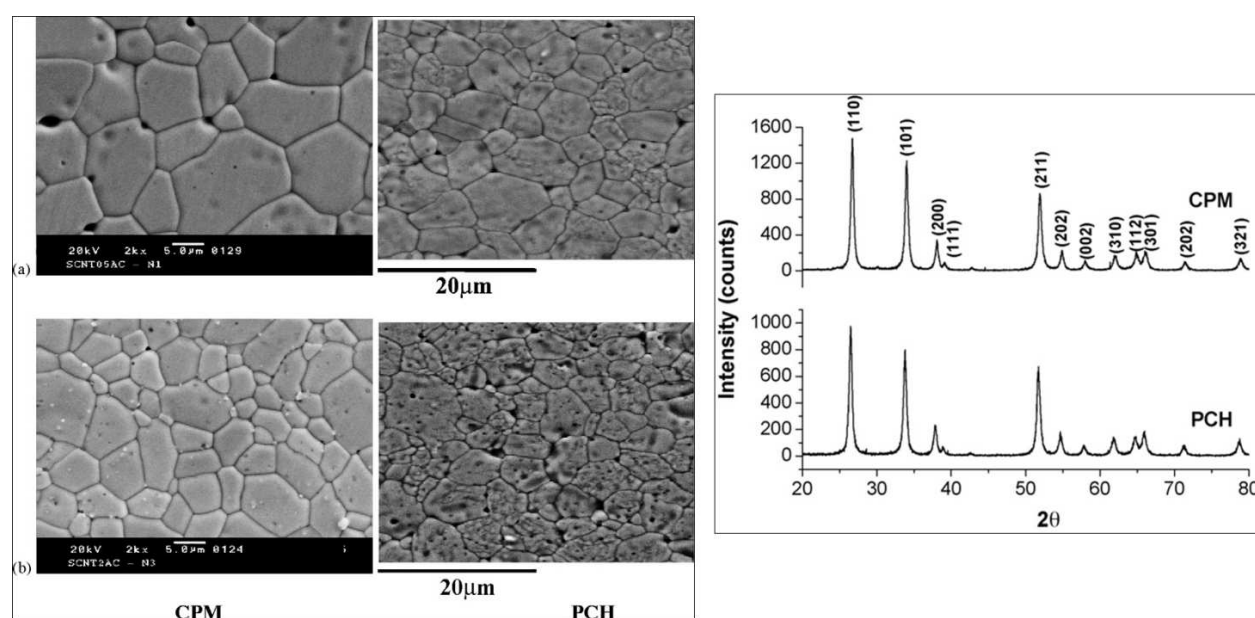

Figure 4. SEM for sintered samples at 1350°C, obtained by CPM and PCH (a) 0.05% Al_2O_3 and (b) 0.1% Al_2O_3. XRD for varistor system whit 0.2% Al_2O_3 synthesized by CPM and PCH [36].

The aluminum concentration also influenced on the electrical properties, as shown in Figure 5, mainly in the breakdown electric field variation that had been related to decreasing of grain size. The samples showed nonlinear coefficient (α) of similar values, but the sample prepared by Pechini method and with 0.2% Al$_2$O$_3$ had the highest value for α (21.7) and the breakdown electric field (due to the smaller grain size).
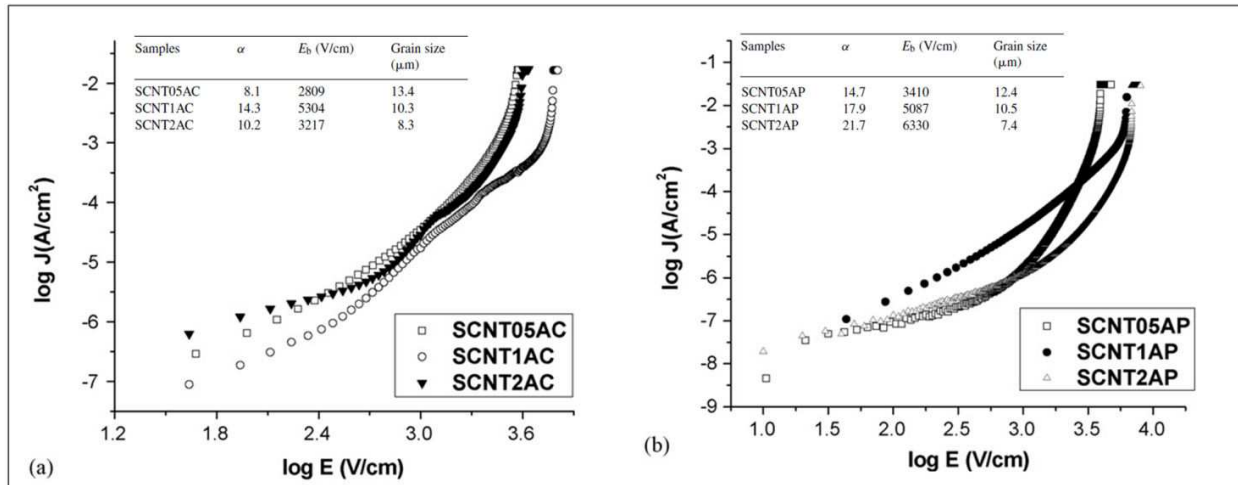

Figure 5. log J *versus* log E curves of samples synthesized by (a) CPM and (b) PCH, sintered at 1350°C [36].

3. New processing step for varistor ceramics

3.1. Microwave sintering

3.1.1. Thermodynamics of sintering

Sintering is the processing step that aims to confer mechanical strength to ceramic or metal powders, shaped by pressing or deposited as films. The process occurs by coalescence of the particles in solid or liquid phase to form a more dense mass. The sintering is an irreversible process and results in decrease of the total free energy of the system. Mathematically, the equation related to total energy of the system is

$$\Delta G = \Delta G_s + \Delta G_i < 0 \tag{10}$$

where ΔG is the total free energy, ΔG_s is the surface free energy, and ΔG_i is the energy of each particular system [37].

3.1.2. Driving force

For the decrease of free energy of the system, there is a force that induces microstructural changes, replacing the contact points between the particles by grain boundaries, closing the pores, densifying, and making the material a hard solid. In addition to the system power

source, the sintering mechanisms are also a contributing factor induced by driving forces. Figure 6 shows the possible forces involved in the sintering process: surface free energy, applied external pressure, and chemical reaction [38].
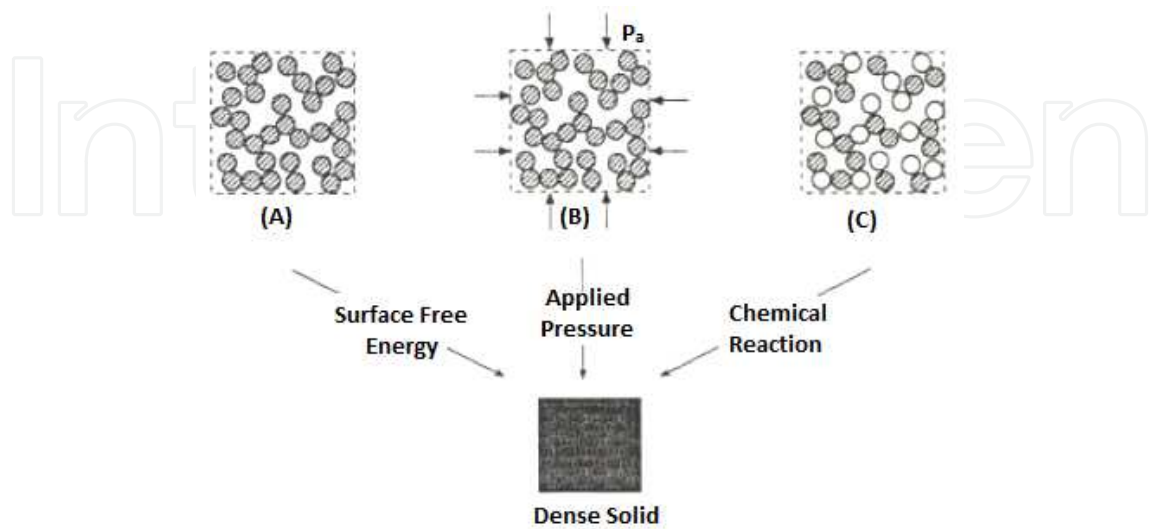

Figure 6. The three main drivers for solid densification: surface free energy, applied pressure, and chemical reaction [38].
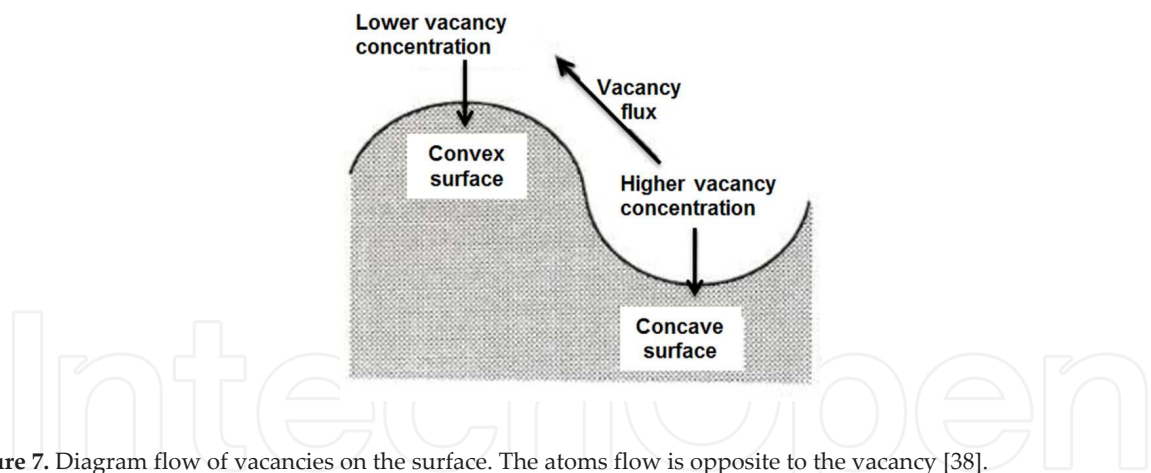

Figure 7. Diagram flow of vacancies on the surface. The atoms flow is opposite to the vacancy [38].

The surface energy is related to the surfaces curve and characterized by vacancies and gaps. The surfaces energy is the main force that sinters the material by mass flow through the region of higher concentration to a lower concentration region where vacancies and gaps, as shown in Figure 7.

The variation of free energy during sintering is represented by Eq. 11:

$$\delta G = \delta \int \gamma_{SS} dA_{SS} + \delta \int \gamma_{SV} dA_{SV} \qquad (11)$$

where the free energy variation depends on the variation on interfacial energy as a function of the surface area. The surface tension solid–solid ($\gamma_{S/S}$) is smaller than the surface tension between vapor-solid ($\gamma_{S/V}$), and the interfacial energy is higher when there are many vacancies in the material, so there is a mass transfer gradient that favors the formation of necks between the particles and the resulting in joint, reducing the solid–vapor area (pore) [37].

3.1.3. Sintering mechanisms

In polycrystalline materials, the mass transport ways that are responsible for sintering are diffusion via crystal lattice, surface diffusion, volume diffusion, plastic flow, and evaporation–condensation. Figure 8 shows all mass transport paths arrive at the point of contact between two particles [38].
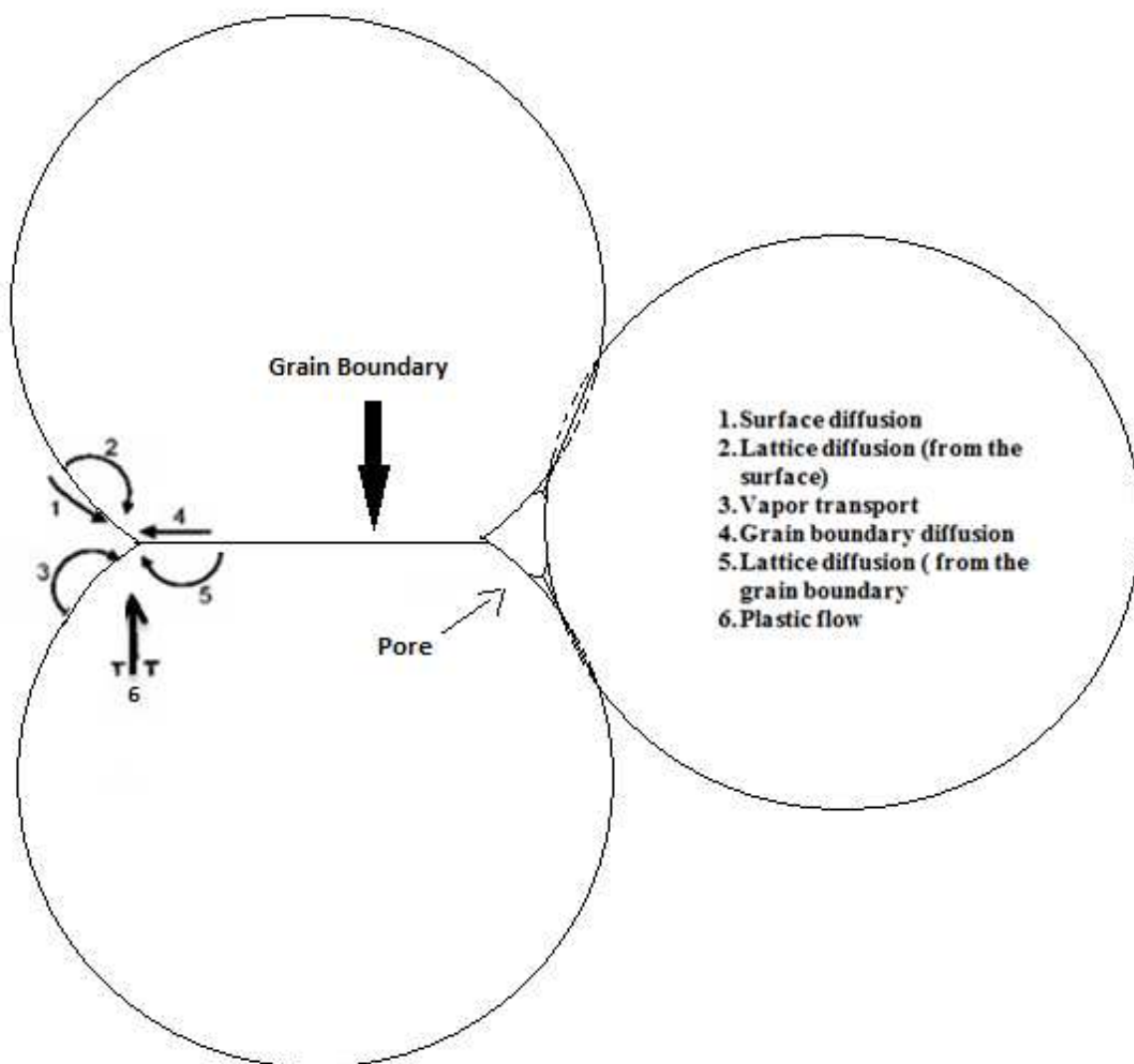

Figure 8. Mass transport mechanism solid and viscous sintering [38].

In Figure 8, the first three mechanisms do not lead to an alignment of the mass centers of the particles and therefore are non-densifying mechanisms. Thus, the mechanisms that start on the volume of material to the neck that increase in the neck and decrease the distance between the particles are densifying mechanisms [39].

3.1.4. Stages of sintering

The sintering mechanisms occur by three successive or simultaneously stages divided into initial, intermediate, and final stages. In some cases, there is the zero stage, which corresponds to particle rearrangement stage for subsequent joining by spot contact called necks [40]. The initial stage consists of particles rounding, formation of necks with low grain growth, and significant reduction in surface area and porosity. This stage progresses until the point where the necks interfere with each other. This stage corresponds to the point where the dihedral angle of equilibrium is reached. For the system with the green density of ~60%, this corresponds to a linear shrinkage of 3% to 5% [36]. It is possible to develop a general equation of the sintering kinetics for the initial stage. The geometric model for the development of this mathematical relationship is illustrated in Figure 9:
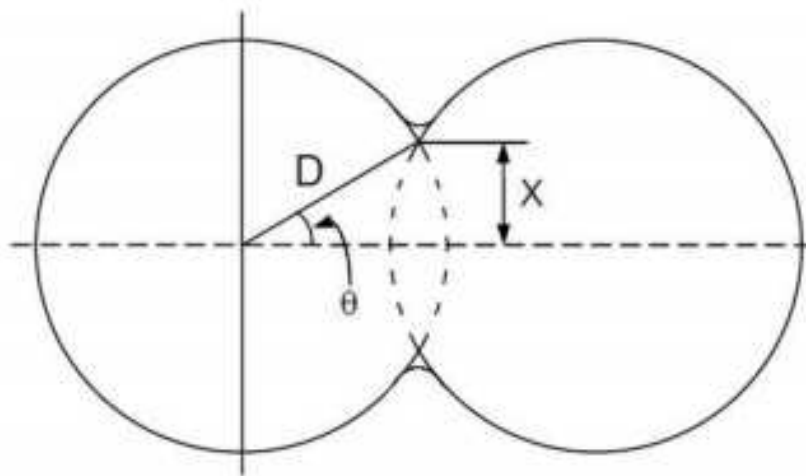

Figure 9. Frenkel's model for early-stage sintering viscous flow [41].

The two spheres of the Frenkel's model use the concept of viscous flow of atoms that relates the vacancy diffusion coefficient D_v, the volume of the atom or vacancy Ω, and vacancy concentration gradient per unit area of the material (dC_v/dx), as shown in the following equation [41]:

$$J_a = \frac{D_v}{\Omega} \frac{dC_v}{dx} \tag{12}$$

Thus, the transported mass volume as a function of time can be given by [41]

$$\frac{dV}{dt} = J_a A_{gb} \Omega \tag{13}$$

were $A_{gb} = 2\pi X \delta_{SV}$ is equal to the cross-sectional area where diffusion occurs, and X is the radius of the neck.

Assuming that the decrease in surface energy of the system is equivalent to the energy dissipated through the material flow, then it is possible to derive several equations relating the radius of the neck and ball as a function of sintering time [38,42]:

$$\left(\frac{X}{a}\right)^m = \frac{H}{a^n} t \tag{14}$$

where m and n are the sintering mechanisms, H is a function that varies with parameters such as diffusion rate, surface tension, atom or vacancy size, and a is the radius of the sphere.

Many aspects can be studied from the kinetic equations, as densification rate, determination of sintering mechanisms, and activation energy. The equation developed by Coble allows to estimate the sintering mechanisms for the initial stage, based on the two spheres Frenkel's model, as indicated in the Eq. 15 [43]:

$$Y^n = k_0 exp\left(\frac{-Q}{RT}\right) t \tag{15}$$

where $n = 1, 2, 3$, or 4, indicating the predominant mechanism of viscous flow, surface diffusion, and diffusion via grain boundary diffusion and via crystal lattice, and Y is the linear shrinkage of the sample, Q is the activation energy, R is the gas constant real, T is the temperature, and t is time.

The intermediate stage initiates densifying mechanisms as volumetric diffusion by crystal lattice in which there is rapid grain growth, shrinkage pore and increased in the density of the material up to ~90% of the theoretical density. Whereas there is grain growth, the model for the initial stage does not fit this stage. The final stage is characterized by the elimination of residual pores with little or no densification, but grain growth is observed. For the determination of sintering mechanisms, intermediate and final stages are used in the model-based grain growth [44]:

$$G^n - G_0^n = k_0 exp\left(\frac{-Ea_b}{RT}\right) t \tag{16}$$

where G is the average grain size, Ea_b is the activation energy for moving contour or grain growth, n is the sintering mechanism when valley 3 is spread via reticulum and 4 is broadcast via grain boundary, and k_0 is a constant that depends on temperature and sintering mechanisms [41,43,44].

3.1.5. Sintering model for thick films

Most of the kinetic studies of SnO$_2$-based ceramic are developed to oxide mixed synthesis compressed into pellets, where significant amounts of mass are used. However, the appearance of thick and thin films makes possible the integration of smaller electric devices, and thus new techniques for the synthesis and deposition of powders on conductive and insulating rigid substrates have been studied.

The sintering of films has been increasingly used for applications in sensors, fuel cells, or photo catalysis that requires porous films [45,46]. This application is based on the fact that sintering occurs on rigid substrates such as viscous flow, wherein the voltage-limiting densification of the material is the force of attraction between the substrate and the deposited material particles [47,48]. The model used for understanding the sintering of thin films is based on Scherer and Garino's studies where the rate of densification of the film is delayed by the substrate, as in Eq. 17 [38,41]:

$$\left(\frac{\dot{\rho}}{\rho}\right)_c = -\left[\frac{1+v_p}{3\left(1-v_p\right)}\right]3\dot{\varepsilon}_f \tag{17}$$

The sintering mechanisms remain the same; however, the densification rate is retarded by tension caused by the substrate, like as the system would be sintered followed viscous sintering mechanism, as with glass.

3.1.6. Microwave × conventional sintering of SnO$_2$-based ceramic

One of the ceramic materials that have been very exploited for its great technological and industrial interest is the SnO$_2$. Its applications are widely focused on sensors, solar cells, and catalysts, i.e., requiring high porosity, since its sintering process is limited to nondensifying mechanisms such as surface diffusion at low temperatures and evaporation–condensation at high temperatures [49–51]. Accordingly, what has been done to induce densifying sintering mechanisms is to cause solid substitution reactions that decrease the free energy by the formation of substitutional defects and vacancies that facilitate material transport during sintering [52].

It is possible to increase the densification of SnO$_2$ by the addition of small amounts of lower valence densifying agents that generate substitutional defects and oxygen vacancies, such as ZnO, CoO, and MnO$_2$, that promote the mass diffusion by solid solution, according to Eqs. 18, 19, and 20 [52,53]:

$$ZnO \xrightarrow{SnO_2} Zn''_{Sn} + V_O^{\bullet\bullet} + O_O^X \tag{18}$$

$$CoO \xrightarrow{SnO_2} Co''_{Sn} + V_O^{\bullet\bullet} + O_O^X \tag{19}$$

$$MnO_2 \xrightarrow{SnO_2} Mn_{Sn}^{''} + V_O^{\bullet\bullet} + O_O^X \tag{20}$$

Also, there is the densification by CuO, Fe$_2$O$_3$, and MnO doping that promotes liquid solution formation [51]. Another way to improve the densification of SnO$_2$-based varistors is to use the microwave as a source of power in the sintering process. According to Hao et al. [53], while conventional sintering occurs as a consequence of surface energy reduction, microwave sintering not only reduces the surface energy but also creates vacancies in the neck [53]. As a consequence of the increase in vacancies in grain necks, the mass flow also enhances in this region, promoting densification. In the case of dielectric materials, the oscillation of the electric field is the only external factor that will cause the internal heating of the material. Thus, the response of the oscillating electric field to the dielectric is determined by $\varepsilon = \varepsilon' + i\,\varepsilon''$, where ε' is a dielectric constant that depends on the medium, and ε'' is the dielectric loss factor; when the material exhibits high dielectric loss, i.e., a high value ε'', the microwave energy is absorbed and converted into heat within the material [54]. When a material has high dielectric loss, the microwave can be directly applied to it; however, a susceptor material must be used. The susceptor absorbs microwave radiation and heats up the first piece so that it reaches its critical temperature, which consists of 40% to 50% of the melting temperature of the material above which has high dielectric losses.

3.2. SnO$_2$ microwave sintering

Sintering mechanisms at Coble initial stage were adjusted to SnO$_2$-based ceramic inserts with 0.95 mol% of ZnO sintered in a microwave oven and compared with results obtained in a conventional oven. The results showed that samples were sintered in a microwave oven to reach 87% after 30 min of sintering at 1050°C and grain size, while in a conventional oven, the density is 67%. It can be seen in Figure 10 by which the sample (a) is in the initial stage of sintering grain size, while in (b) indicating the morphology of the grains is already in intermediate sintering mechanism.
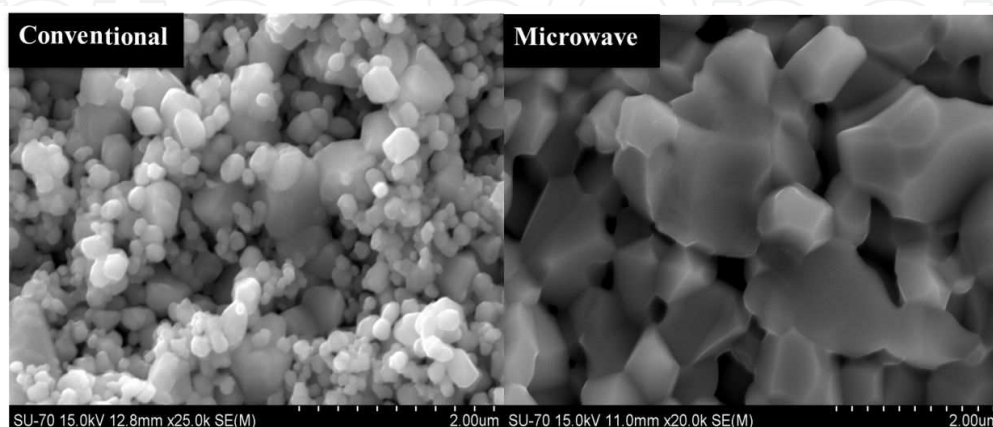

Figure 10. SEM of sintered samples in (a) conventional oven and (b) microwave oven, at 1050°C/30 min (by authors).

The sample sintered in a conventional oven showed a linear shrinkage of 5% and had an activation energy of 325 kJ/mol with predominant mechanisms at this early stage: structural rearrangement of particles, diffusion via crystal lattice, and surface diffusion, while samples sintered in microwave oven showed an activation energy of 111 kJ/mol and mechanisms as broadcast via crystalline reticulum. Figure 11 shows that there was a change sintering mechanisms for conventional sintering since there is a rate change in linear shrinkage rate of the material, whereas for microwave sintering the heating rate was rapid and lower temperature which does not inhibit sintering mechanisms densifying.
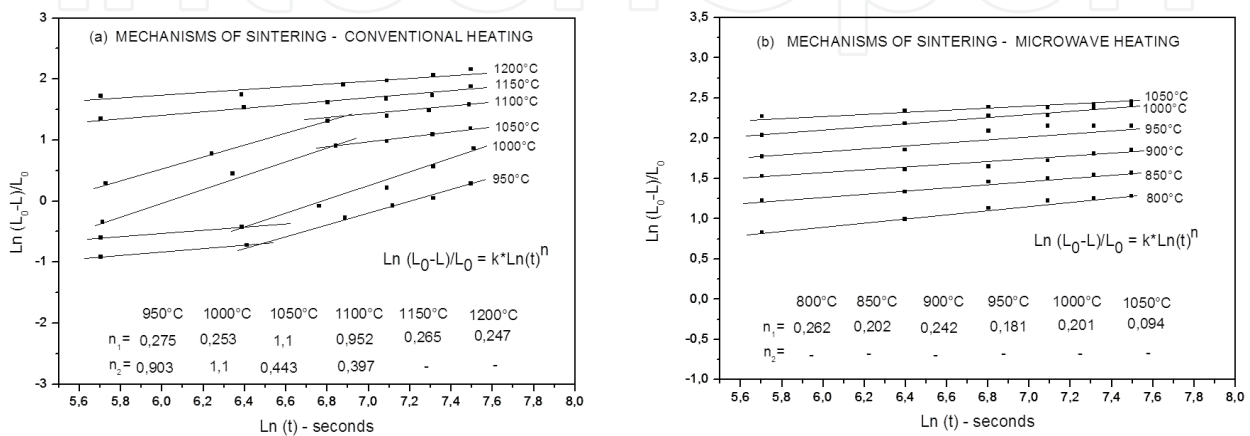

Figure 11. Curves of Ln(Y) *versus* Ln(t) with temperature as a parameter for obtaining the coefficients of sintering at initial stage, for SnO_2 samples (doped with 0.95 mol% of ZnO) sintered in (a) oven conventional and (b) microwave oven (by authors).

The direct relationship between the grain growth and the increasing density for the samples subjected to microwave and conventional heating are shown in Figure 12. With their respective error bars, it may be said that for about the same density of 88% of the samples, the mean grain size for the sintered sample in a microwave oven at 1050°C for 30 min is 1.2 μm, while that for the samples sintered in a conventional oven at 1300°C/30 min is 1.8 μm, and this difference increases even more because it enters the final sintering stage, which is when the grains grow more sharply, so the grain size is increased to about 3 μm. The reduced grain samples sintered in a microwave oven results in more grain boundaries to increase the mechanical strength and modifying the electrical properties of the material.

3.3. Thick films varistor obtained by electrophoretic deposition

Lustosa et al. [55] conducted a study on thick films of SnO_2-based nanoparticles and their electrical properties. The ceramic powder with composition 98.95 mol% SnO_2 + 1 mol% ZnO + 0.05 mol% Nb_2O_5 was synthesized by Pechini method, calcined in a muffle furnace, submitted to milling in the Attritor mill and to the separation of particles by gravimetry. After separation for use of the smaller particles, one ethylic aliquot containing SnO_2 powder was taken to an electrophoretic deposition system (Figure 13) for obtain the films. In sequence, the films were submitted to sintering in a microwave oven at 1000°C/40 min. In order to improve the varistor
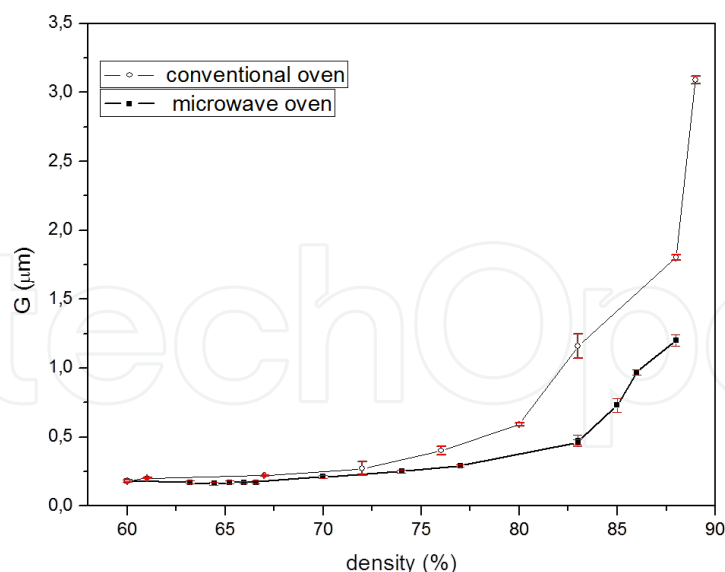
Figure 12. Evolution of grain size as a function of the calculated density of the samples sintered in a conventional oven and a microwave oven at a temperature of 800 °C to 1050 °C [by authors].

property, a Cr^{3+} ion deposition was carried out (also by electrophoresis) on films surface, and then the samples were submitted to different heat treatment for the diffusion of cations in grain boundary region. Figure 14 shows the sintered film, which had a low porosity, homogeneous thickness to the full extent of the film. The chromium addition is known to improve the properties of a varistor system by acting on defect formation at grain boundary region and increase the potential barrier parameter.
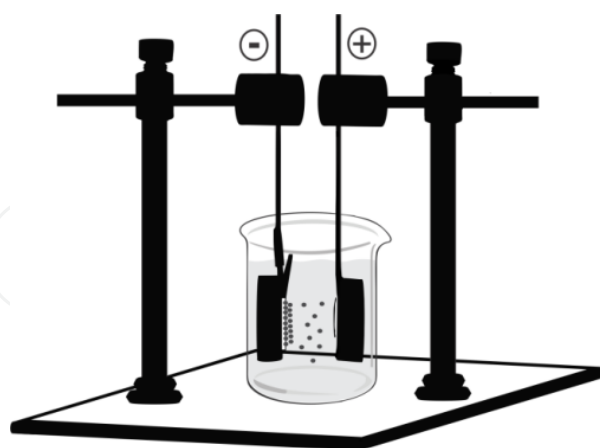

Figure 13. Electrophoretic system for deposition of SnO$_2$-based particles (by authors).

After the heat treatment for Cr^{3+} diffusion, the films were taken to the electrical characterization. From the varistor responses, shown in Figure 15, it was observed that the heat treatment used after the chromium deposition influenced the improvement of the nonlinear coefficient of the samples. All films had lower rupture voltage less than 65 V and a low leakage current.
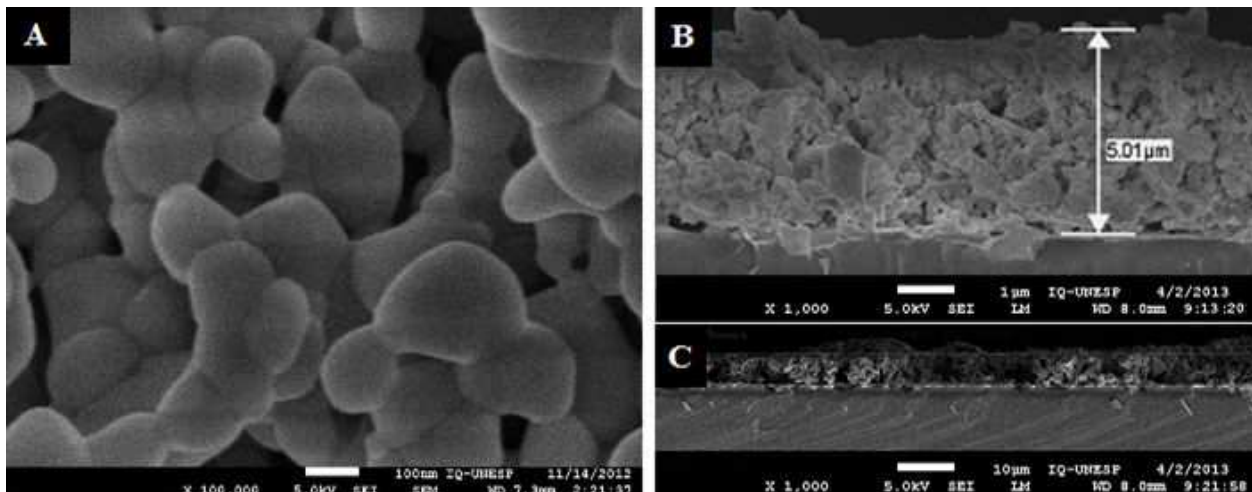
Figure 14. SEM of the film deposited by electrophoresis and sintered at 1000 °C/40 min: (a) top vision; (b) and (c) different magnifications of cross-sectional vision [55].
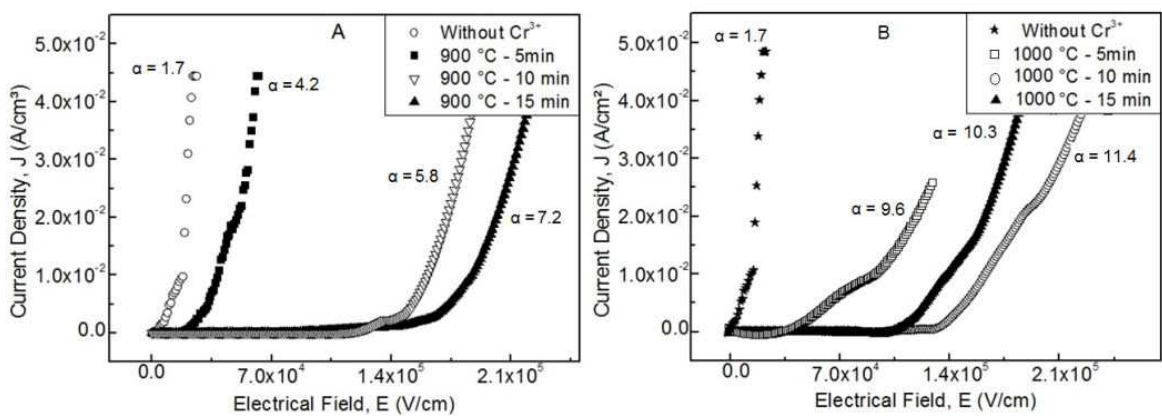

Figure 15. Graphs of current density *versus* electric field: (a) for films without Cr³⁺ and films thermally treated at 900 °C and (b) films thermally treated at 1000 °C after the Cr³⁺ deposition [55].

## 4. Network modifiers that promote properties of SnO$_2$-based varistor

The addition of crystal lattice modifiers to SnO$_2$ matrix is required because in the SnO$_2$ sintering process, there is a predominance of mass transport mechanisms (evaporation and condensation), which leads to coalescence and grain growth, which hinder densification. Densification is a precondition to obtain the varistor properties since the phenomena involved in the formulation of non-ohmic properties occur in the grain boundary region. Thus, the studies are carried out to understand the doping effect on the sintering and densification, electrical conductivity, and non-ohmic properties of SnO$_2$-varistor. The defects generated by modifying agents are of Frenkel type (generators of interstitial ion) and Schottky type (generators of vacancies) and are responsible for the formation and modification of the potential barrier in the grain boundaries [1,56,57].

The addition of bivalent metals such as CoO [58], ZnO [59], and CuO [60,61] is made to enhance the densification because these cations act as acceptors of electrons and replace the tin ions in crystal lattice, creating oxygen vacancy defects that promote mass diffusion in the network and promoting densification, according to Eq. 21 [58]:

$$MO \xrightarrow{SnO_2} M_{Sn}^{''} + V_O^{\bullet\bullet} + O_O^X \qquad (21)$$

The $M_{Sn}^{''}$ defect types present in the grain boundary region trap the electrons released by other types of modifiers and create a potential barrier in the grain boundary region.

The electrical conductivity of the varistor system can be improved with the addition of pentavalent ions as Sb$_2$O$_5$ [62], Nb$_2$O$_5$ [1], and V$_2$O$_5$ [63], which act as electron donors to the crystal lattice, resulting in electron concentration and tin vacancies, as demonstrated in Eq. 22 [1,62]:

$$D_2O_5 \xrightarrow{SnO_2} 2D_{Sn}^{\bullet} + 2e' + 4O_O^X + \tfrac{1}{2}O_{O(g)}^X \qquad (22)$$
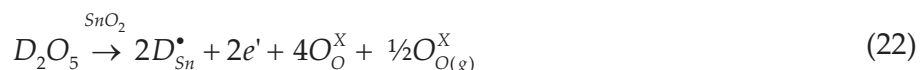
Trivalent cations that act as acceptors of electrons are added to SnO$_2$ crystal lattice, such as chromium [63–65], ytterbium [67], and scandium [68], which were used to improve the varistor properties of the system. The segregation of these ions in the grain boundary potential barrier increases the resistivity values and causes the improvement of nonlinear coefficient due to the higher adsorption of electron acceptor species on the grain boundary surface, increasing the barrier height potential and decreasing the conductivity, as demonstrated in Eq. 23 [57,58,67]:

$$M_2O_3 \xrightarrow{SnO_2} 2M_{Sn}^{'} + V_O^{\bullet\bullet} + 3O_O^X \qquad (23)$$

There are many papers available in the literature [56–58,61–63,66–70], which studied the influence of doping agent into the tin oxide matrix ceramic. The possible microstructural, morphological, and varistor property changes that may occur with the addition of certain elements are searched.

4.1. Effect of Ca, Ba, Sr addition on Co, Sb-doped SnO$_2$ varistors

Aguilar-Martínez et al. [69] investigated the effect of calcium (sample named SCa), barium (sample named SBa), and strontium (sample named Sr) additions on the microstructure and electrical properties of SnO$_2$-Co$_3$O$_4$-Sb$_2$O$_5$ ceramic varistors.

By XRD analysis, it should be noted that the concentrations of dopants added (SbO, CaO, Ba, and SrO) were too small to be detected by the X-ray equipment. The microstructure of the samples was characterized by scanning electron microscopy. As shown Figure 16, it was found

that the addition of strontium and calcium promotes densification and grain growth. The addition of BaO leads to a significant alteration of microstructure, changing the grain size and the morphology of grains from a nearly round shape to smaller and elongated grains. Barium addition causes increase of porosity, reduction of grain size, and changes in the grain morphology (from approximately equiaxed to elongated grains) [69].
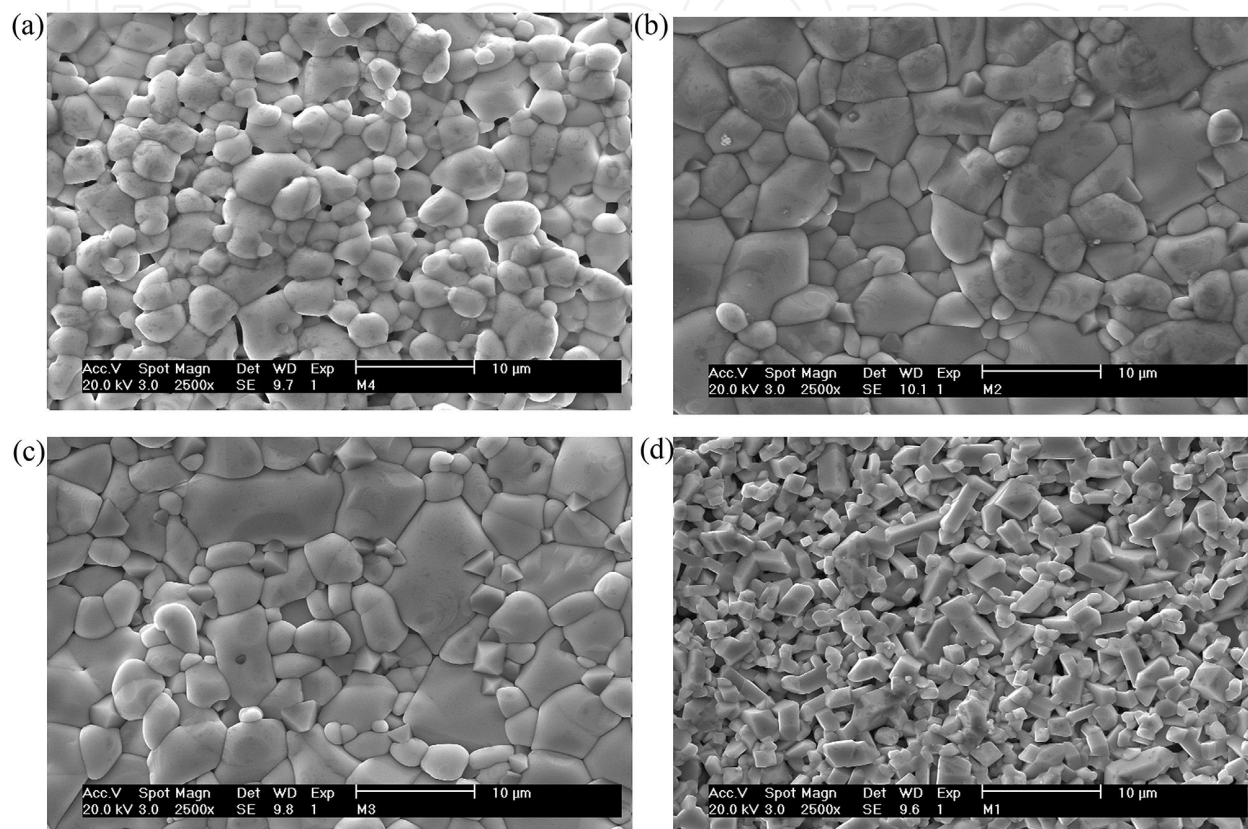

Figure 16. SEM images of the as-sintered surfaces of SnO_2-based varistors: (a) S, (b) SCa, (c) SSr, and (d) SBa [69].

Since electrical conduction in SnO_2-based varistor ceramics is controlled by the grain-boundary barriers, the observed fact (the significant grain growth in a SnO_2-system with SrO and CaO added) suggests that Sr and Ca materials are more suitable for low-voltage varistor preparation. The current–voltage curves of all prepared ceramic samples are nonlinear behavior. Figure 17 shows graphs of current density versus electric field for ceramics with and without additions sintered at 1350 °C [69].

Ceramics with calcium addition exhibit the lowest electric field at a fixed current density (10^{-3} A cm^{-2}). The addition of strontium shows a similar effect on microstructure and current–voltage characteristics. However, the BaO addition showed that low-field conductivity is slightly lower with respect to the reference material, but the high-field part remains unchanged. This behavior may be attributed to the resulting microstructure. Despite the grain morphology and porosity, the samples S (only Co an Sb as dopants), SCa, and SBa showed
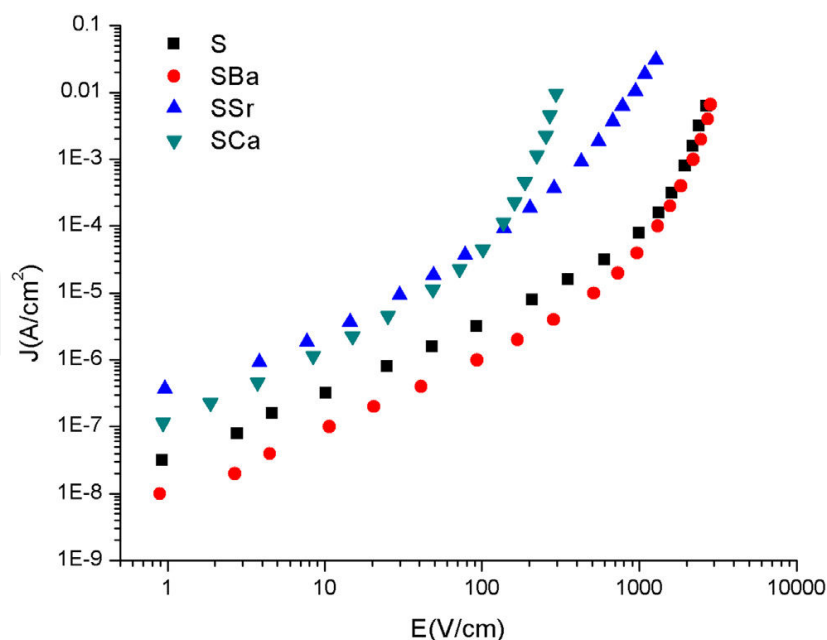
Figure 17. J *versus* E characteristic plots for all samples [69].

nonlinear coefficients of 5.7, 5.0, and 4.9, respectively, higher than the value for sample SSr (nonlinear coefficient of 2.7) [69].

4.2. Effect of Er addition on Co, Nb-doped SnO$_2$ varistors

The addition of Er$_2$O$_3$(Co, Nb)-doped SnO$_2$ was studied by Qi et al. [70] at different concentrations (0.1, 0.5, 1, and 2 mol%) and different temperatures of sintering (1250 °C, 1300 °C, and 1350 °C for 1 h).The XRD analysis carried out by the authors did not show evidence of the second phase formation into the SnO$_2$-rutile crystalline phase. The SEM micrographs of the varistors prepared are in Figure 18, showing the decreases of grain size associated with the increase of Er$_2$O$_3$ concentration into ceramic matrix. Also, the decreases of grain size occur with lower temperature of sintering. With the addition of 2.0 mol% of Er$_2$O$_3$ modifier agent, the SnO$_2$ grain size was reduced from 12.9 μm to 6.5 μm when the sample sintered at 1350°C for1 h, from 9.7 μm to 3.7 μm when sample was sintered at 1300°C for 1 h, and from 6.8 μm to 2.4 μm when samples were sintered at 1250°C for 1 h.

Figure 19 shows the plots of applied electric field versus current density for different concentrations of Er$_2$O$_3$ sintered at 1350 °C, 1300 °C, and 1250 °C during 1 h. It was observed from Figure 19 that the threshold voltage of the SnO$_2$-based varistors increased significantly from 305 V mm^{-1} to 1083 V mm^{-1} with increasing Er$_2$O$_3$ concentrations over the range of 0–2.0 mol % sintered at 1350°C during 1 h and from 1083 V mm^{-1} to 2270 V mm^{-1} with decreasing sintered temperatures from 1350°C to 1250°C during1 h. Only the samples sintered at 1300 °C have decrease on nonlinear coefficient with Er$_2$O$_3$ addition. There is no observed significant change on height of the potential barrier for samples sintered ate 1250°C and 1300 °C.
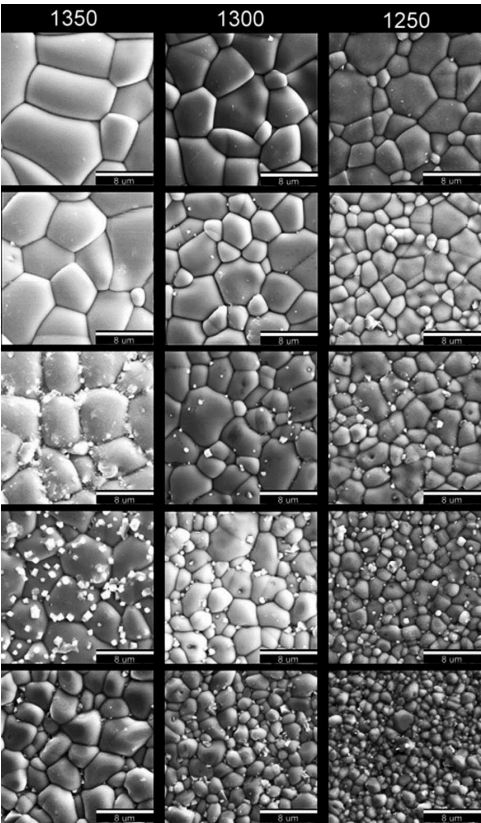
Figure 18. Microstructure variation of the SnO$_2$-based varistor system sintered at 1350 °C, 1300 °C, and 1250 °C during 1 h with the composition (all in mol%): 100SnO$_2$ + 0.75Co$_2$O$_3$ + 0.1Nb$_2$O$_5$ + xEr$_2$O$_3$: (from top to bottom) x = 0.0, x = 0.1, x = 0.5, x = 1.0, x = 2.0 [70].
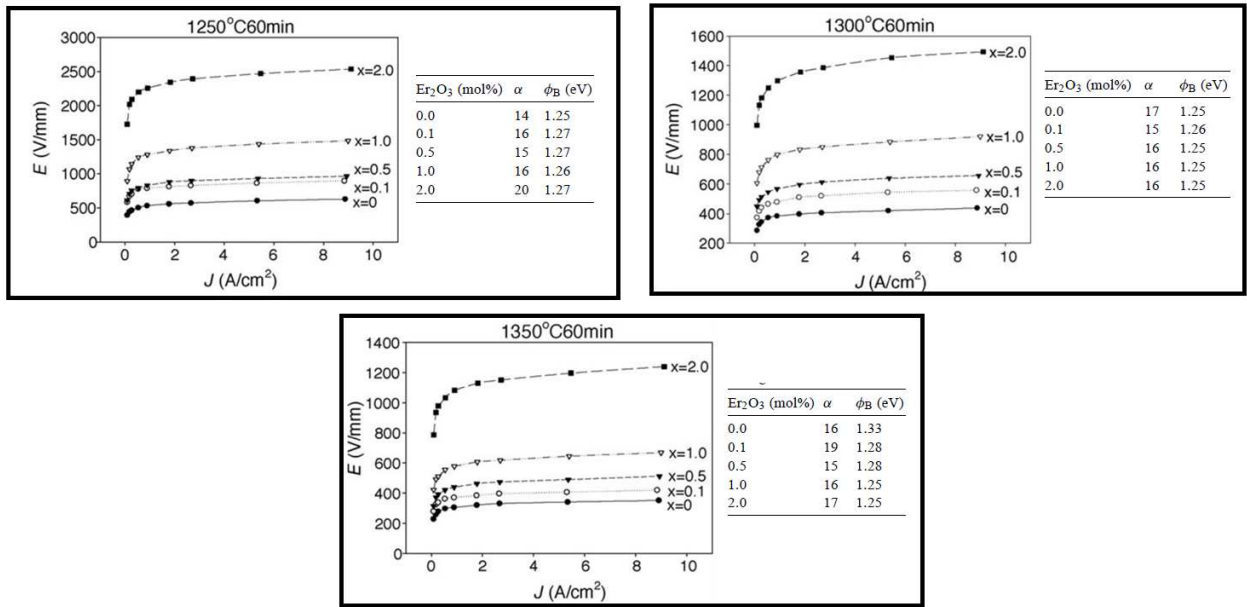

Figure 19. E versus J curves for the SnO$_2$-based varistor system sintered at different temperatures during 1 h with the composition (all in mol%) 100SnO$_2$ + 0.75Co$_2$O$_3$ + 0.1Nb$_2$O$_5$ + xEr$_2$O$_3$ (x ranging from 0.0 to 2.0) [70].

5. Conclusions

The study of SnO$_2$-based varistor systems is recent, so a huge amount of published papers do not exist. Research involving the material is mostly related to the understanding of the influence of dopants on densification materials prepared by mixing oxide and the change in the parameters of the potential barrier formed at grain boundary region, which is directly related to the nonlinear coefficient and determines the quality of varistor ceramics. The bivalent metals (Ba^{2+}, Ca^{2+}, Co^{2+}, Zn^{2+}, and others) have proven action as a densifying agent since the defects generated by their addition to the ceramic matrix assist in mass diffusion. The addition of trivalent ions (Cr^{3+}, Er^{3+}, and others) causes the increase of nonlinearity coefficient due to the higher adsorption electron acceptor species on the surface of the grain boundary and thus causing a reduction in conductivity of the material. The new methodologies for the chemical synthesis of ceramic powder promote the homogeneous distribution of dopants into the ceramic matrix and reduce segregation and the formation of secondary phases, confirmed by XRD analysis, which are harmful factors on the electrical properties of the varistor and facilitate the integration of the material in today's electronic devices electrical protection. The use of microwave oven is a new processing step aimed to reduce the time and temperature of sintering step and can be considered a promising procedure for the varistors production. The preparation of varistors as film emerges as a new possibility in order to facilitate integration of this material in electronic circuits.

Acknowledgements

Author details

Glauco M.M.M. Lustosa, Natalia Jacomaci, João P.C. Costa, Gisane Gasparotto, Leinig A. Perazolli and Maria A. Zaghete[*]

*Address all correspondence to: zaghete@iq.unesp.br

Interdisciplinary Laboratory of Electrochemistry and Ceramics (LIEC), Chemistry Institute– UNESP, Araraquara/SP, Brazil

References

[1] Pianaro SA, Bueno PR, Olivi P, Longo E, Varela JA. Electrical properties of the SnO$_2$-based varistor. J Mater Sci Mater El. 1998;9:159–165. DOI: 10.1023/A:1008821808693

[2] Furtado JGM. Correlações entre fenômenos de grão e de contornos de grão e o desempenho de cerâmicas varistoras [thesis]. Rio de Janeiro: Universidade Federal do Rio de Janeiro; 2005.

[3] Matsuoka M. Nonohmic properties of zinc-oxide ceramics. Jpn J Appl Phys. 1971;10:736–746.DOI:10.1143/JJAP.10.736

[4] Bartkowiak M, Comber MG, Mahan GD. Energy handling capability of ZnO varistors. J Appl Phys. 1996;79:8629–8633.DOI: 10.1063/1.362484

[5] Castro MS, Benavente MA, Aldao CM. Degradation in ZnO varistor. J Phys Condens Mater. 1993;5:341–342.DOI: 10.1088/0953-8984/5/33A/125

[6] Xuetong Z, Jianyin L, Huan L, Shengtao L. The impulse current degradation of ZnO varistor ceramics. Proceedings of 2011 International Conference on Electrical Insulating Materials (ISEIM),2011;no:43–46. DOI: 10.1109/ISEIM.2011.6826272

[7] Pianaro SA, Bueno PR, Longo E, Varela JA. A new SnO_2-based varistor system. J Mater Sci Lett. 1995;14:692–694. DOI: 10.1007/BF00253373

[8] Gupta TK. Application of zinc oxide varistors. J Am Ceram Soc. 1990;73:1817–1840. DOI: 10.1111/j.1151-2916.1990.tb05232.x

[9] Levinson LM, Philipp HR. ZnO varistors for transient protection. IEEE Trans Parts HybPac. 1977;13:338–343. DOI: 10.1109/TPHP.1977.1135218

[10] Pianaro SA, Bueno PR, Longo E, Varela JA. Microstructure and electric properties of a SnO_2 based varistor. Ceram Int. 1999;25:1–6. DOI: 10.1016/S0272-8842(97)00076-X

[11] He J, Zeng R, Chen S, Tu Y. Thermal characteristics of high voltage whole-solid insulated polymeric ZnO surge arrester. IEEE Trans Power Deliver. 2003:18:1221–1227. DOI: 10.1109/TPWRD.2003.817492

[12] Santos P A. A importância do tempo de sinterização sobre as propriedades elétricas de varistores de SnO_2 [thesis]. Ponta Grossa: Universidade Estadual de Ponta Grossa; 2004.

[13] Prisching D, Pecina AH. Temperature behavior of ZnO varistors before and after post sintering heat treatment. Mater Let. 2000;43:295–302. DOI: 10.1016/S0167-577X(99)00277-3

[14] Bueno PR, Pianaro SA, Pereira EC, Varela JA. Investigation of the electrical properties of SnO_2 varistor system using impedance spectroscopy. J Appl Phys. 1998;84:3700–3705. DOI: 10.1063/1.368587

[15] Oliveira MM, Rengel JHG, Sousa VC, Leite ER, Longo E, Bueno PR, Varela JA. Desenvolvimento devaristores à base de SnO_2 para aplicação em redes de alta tensão. Cerâmica. 2006;54:149–154. DOI: 10.1590/S0366-69132006000300007

[16] Clarke DR. Varistor ceramics. J Am Ceram Soc. 1999;82:485-502.DOI: 10.1111/j. 1151-2916.1999.tb01793.x

[17] Moulson A, Herbert JM. Electroceramics: Materials, Properties and Applications. 2nd ed. London: Chapman & Hall; 2003. 576 p. DOI:10.1002/0470867965

[18] He J, Peng Z, Fu Z, Wang Z, Fu X. Effect of ZnO doping on microstructural and electrical properties of SnO$_2$-Ta$_2$O$_5$ based varistor. J Alloys Compd. 2012;528:79–83. DOI: 10.1016/j.jallcom.2012.02.172

[19] Feng H, Peng Z, Fu X, Fu Z, Wang C, Qui L, Miao H. Effect of SnO$_2$ doping on microstructural and electrical properties of ZnO-Pr$_6$O$_{11}$ based varistor ceramics. J Alloys Compd. 2011;509:7175–7180. DOI: 10.1016/j.jallcom.2011.04.042

[20] Glot AB, Gaponov AV, Sandoval-García AP. Electrical conduction in SnO$_2$ varistors. Physica B. 2010;405:705–711. DOI: 10.1016/j.physb.2009.09.091

[21] Bastami H, Taheri-Nassaj E. (Co, Nb, Sm)-doped tin dioxide varistor ceramics sintered using nanopowders prepared by coprecipitation method. J Am Ceram Soc. 2011;94:3249–3255. DOI: 10.1111/j.1551-2916.2011.04467.x

[22] Gupta TK, Carlson WG. A grain-boundary defect. Model for instability/stability of a ZnO varistor. J Mater Sci. 1985;20:3487–3900. DOI: 10.1007/BF01113755

[23] Leite ER, Varela JA, Longo E. A new interpretation for the degradation phenomenon of ZnO varistor. J Mater Sci. 1992;27:5325–5329. DOI: 10.1007/BF00553413

[24] Wang JF, Su WB, Chen HC, Wang WX, Zang GZ. (Pr, Co, Nb)-doped SnO$_2$ varistors ceramics. J Am Ceram Soc. 2005;88:331–334. 10.1111/j.1551-2916.2005.00095.x

[25] Felix AA, Orlandi MO, Varela JA. Schottky-type grain boundaries in CCTO ceramics. Solid State Commun. 2011;151:1377–1381. DOI: 10.1016/j.ssc.2011.06.012

[26] Frenkel J. On pre-breakdown phenomena in insulator and electronic semi-conductor. Phys Rev. 1983;53:647–652. DOI: 10.1103/PhysRev.54.647

[27] Bwrnasconi J, Klein HP, Knecht B, Strassler S. Zinc oxide based varistor: a possible mechanism. Solid State Commun. 1976;20:1053–1056. DOI: 10.1016/0038-1098(77)90351-9

[28] Srague Electric Co. (USA). M. P. Pechini. Method of preparing lead and alkaline titanates and niobates and coating method using the same to form a capacitor. U.S. patent no. 3330697; 1967.

[29] Tang FQ, Uchikoshi T, Sakka Y. Electrophoretic deposition behavior of aqueous nanosized zinc oxide suspensions. J Am Ceram Soc. 2002;85:2161–2165. DOI: 10.1111/j.1151-2916.2002.tb00428.x

[30] Stojanovic BD, Mitic V, Pejovic V, Vijatovic MM, Zaghete MA. Screen printed PLZT thick films prepared from nanopowders. J Eur Ceram Soc. 2007;27:4359–4362. DOI: 10.1016/j.jeurceramsoc.2007.02.170

[31] Lisboa Filho PN, Zenatti A, Casali GM, Paskocimas CA, Ortiz WA, LeiteER, Longo E. Magnetic behavior at low temperatures of Ti oxide polycrystalline samples. J Sol-Gel Sci Technol. 2002;24:241–245. DOI: 10.1023/A:1015336712094

[32] Magalhães EC. Propriedades Ópticas de Filmes Finos de Dióxido de Estanho Puro e Dopado com Flúor [thesis]. Salvador: Universidade Federal da Bahia; 200l.

[33] Sabila LF. Interação do complexo luminescente [Eu(tta)$_3$] com sílica mesoporosa [thesis]. Ilha Solteira: Universidade Estadual Paulista; 2009.

[34] Husing N, Schubert U. Aerogels—Airy Materials: Chemistry, Structure, and Properties. Angew Chem Inter Ed. 1998;37:22–45. DOI: 10.1002/(SICI)1521-3773(19980202)37:1/2<22::AID-ANIE22>3.0.CO;2-I

[35] Shubert H, Petzow G. Preparation and characterization of ceramic powders. In: Shigueyki Somiya editor. Advanced Ceramics III. 1st ed. Netherlands: Springer; 1990. p. 45–56. DOI: 10.1007/978-94-009-0763-8_3

[36] Mosquera A, Rodríguez-Páez JE, Varela JA, Bueno PR. Synthesis of SnO$_2$ by chemical routes and its use in varistors production. J Eur Ceram Soc. 2007;27:3893–3896. DOI: 10.1016/j.jeurceramsoc.2007.02.056

[37] Shi JL. Solid state sintering of ceramics: pore microstructure models, densification equations and applications. J Mater Sci. 1999;34:3801–3812. DOI: 10.1023/A: 1004600816317

[38] Rahaman MN. Sintering of Ceramics. 1st ed. Boca Raton: CRC Press. 2007. 388 p. ISBN-10: 0849372860

[39] Rahaman MN. Ceramic Processing and Sintering. 2nd ed. New York: Handcover; 2003. 875 p. ISBN-10:0824709888

[40] Senos AMR, Vieira JM. Pore size distribution and particle rearrangement during sintering. In: P. Duran, J.F. Fernandez, editors.3rd EuroCeramics. San Lorenzo: Faenza Editrice Iberica; 1993. p. 821–826.ISBN-10: 848768307X

[41] Jamin CC. Constrained Sintering of Patterned Ceramic Films on Stiff Substrates [thesis]. Darmstadt: Technischen Universität Darmstadt; 2014.

[42] German RM. Sintering Theory and Practice. 1st ed. New York: Willey. 1996, 568p. ISBN: 978-0-471-05786-4

[43] Coble RL. Effects of particle-size distribution in initial-stage sintering. J Am Ceram Soc. 1973;56:461–466. DOI: 10.1111/j.1151-2916.1973.tb12524.x

[44] Kim J, Kimura T, Yamaguchi ET. Sintering of zinc oxide doped with antimony oxide and bismuth oxide. J Am Ceram Soc. 1989;72:1390–1395. DOI: 10.1111/j. 1151-2916.1989.tb07659.x

[45] Wang CM, Thevuthasan S, Gao F, McCready DE, Chambers SA, Peden CHF. Inter-face characteristics of iso-structural thin film and substrate pairs. Nucl Instrum Meth B. 2003;207:1–9. DOI: 10.1016/S0168-583X(03)00512-3

[46] Thomas B, Skariah B. Spray deposited Mg-doped SnO$_2$ thin film LPG sensor: XPS and EDX analysis in relation to deposition temperature and doing. J Alloy Compd. 2015;625:231–240. DOI: 10.1016/j.jallcom.2014.11.092

[47] Shishun Q, Ruzhong Z, Zhaosheng M. Densification behavior and microstructure evolution of evolution of LTCC film constrained by rigid substrate. Key Eng Mat. 2015;633:93–97. DOI: 10.4028/www.scientific.net/KEM.633.93

[48] Kim JS, Rudkin RA, Wang X, Atkinson A. Constrained sintering kinetics of 3YSZ films. J Eur Ceram Soc. 2011;31:2231–2239. DOI: 10.1016/j.jeurceramsoc.2011.05.044

[49] Bueno PR, Oliveira MR, Santos C, Longo E, Tebcherami SM, Varela JA. Varistores à base de SnO$_2$: estado da arte e perspectivas. Cerâmica. 2000;46:125–130. DOI: 10.1590/S0366-69132000000300002

[50] Varela JA, Perazolli LA, Cerri ER, Leite E, Longo E. Sinterização de óxido de estanho e suas aplicações em eletrônica e no processamento de vidros ópticos de alta pureza. Cerâmica. 2001;47:117–123. DOI: 10.1590/S0366-69132001000200010.

[51] Cerri JA, Leite ER, Gouvêa D, Longo E, Varela JA. Effect of cobalt (II) oxide and man-ganese (IV) oxide on sintering of tin (IV) oxide. J Am Ceram Soc. 1996;79:799–804. DOI: 10.1111/j.1151-2916.1996.tb07949.x

[52] Perazolli LA, Giraldi TR, Biscaro RS, Varela JA, Longo E. Improved densification of SnO$_2$ by doping with ZnO. Sinter Sci Technol. 2000;13:117–122.

[53] Hao HS, Xu LH, Huang Y, Zhang XM, Xie ZP. Kinetics mechanism of microwave sin-tering in ceramic materials. Sci China Ser E: Tech Sci. 2009;52:2727–2731. DOI: 10.1007/s11431-008-0217-3

[54] Żymelka D, Saunier S, Goeuriot D, Molimard J. Densification and thermal gradient evolution of alumina during microwave sintering at 2.45 GHz. Ceram Int. 2013;39:3269–3277. DOI: 10.1016/j.ceramint.2012.10.015

[55] Lustosa GMMM, Costa JPC, Perazolli LA, Stojanovic BD, Zaghete MA. Electropho-retic deposition of (Zn, Nb)SnO$_2$-films varistor superficially modified with Cr^{3+}. J Eur Ceram Soc. 2015;35:2083–2089. DOI: 10.1016/j.jeurceramsoc.2015.01.022

[56] Leite DR, Cilense M, Orlandi MO, Bueno PR, Longo E, Varela JA. The effect of TiO$_2$ on the microstructural and electrical properties of low voltage varistor based on

(Sn,Ti)O$_2$ ceramics. Phys Status Solidi A. 2010;207:457–461. DOI: 10.1002/pssa.200925304

[57] Bacelar WK, Bueno PR, Leite ER, Longo E, Varela JA. How Cr$_2$O$_3$ influences the microstructure and nonohmic features of the SnO$_2$(Co$_x$, Mn$_{1-x}$)O-based varistor system. J Eur Ceram Soc. 2006;26:1221–1229. DOI: 10.1016/j.jeurceramsoc.2005.01.051

[58] Brankovic G, Brankovic Z, Bavolos MR, Cilense M, Varela JA. Influence of the common varistor dopants (CoO, Cr$_2$O$_3$ and Nb$_2$O$_5$) on the structural properties of SnO$_2$ ceramics. Mater Charact. 2004;52:243–241. DOI: 10.1016/j.matchar.2002.11.001

[59] Perazolli LA, Gasparotto Gisane, Jacomaci N, Ruiz M, Zaghete MA, Foschini CR, Aguiar EC, Varela JA. SnO$_2$ dense ceramic microwave sintered with low resistivity. Mater Sci Appl. 2012;3:272–280. DOI: 10.4236/msa.2012.35040

[60] Wang CM, Wang JF, Zhao Y, Su WB. Effects of copper oxide on the microstructural morphology and electrical properties of tin oxide-based varistor ceramics. J Phys D Appl Phys. 2006;39:1684–1689. DOI: 10.1088/0022-3727/39/8/031

[61] Gaponov AV, Glot AB. Electrical properties of SnO$_2$ based varistor ceramics with CuO addition. Mater Sci-Mater El. 2010;21:331–337. DOI: 10.1007/s10854-009-9916-1

[62] Mazalli IO, Las WC, Cilense M. The effect of preparation method and Sb content on SnO$_2$-CuO sintering. J Mater Sci. 2003;38:3325–3330. DOI: 10.1023/A:1025102524795

[63] Gaponov AV, Glot AB, Ivon AI, Chack AM, Jimenes-Santana G. Varistor and humidity-sensitive properties of SnO$_2$-Co$_3$O$_4$-Nb$_2$O$_5$-Cr$_2$O$_3$ ceramics with V$_2$O$_5$ addition. Mater Sci Eng B. 2007;459:76–84. DOI: 10.1016/j.mseb.2007.10.003

[64] Wang, WX, WangJF, Chen HC, Su WB, Zang GZ. Effects of Cr$_2$O$_3$ on the properties of (Co, Nb)-doped SnO$_2$ varistors. Mater Sci Eng B. 2003;9:470–474. DOI: 10.1016/S0921-5107(02)00477-4

[65] Aguilar-Martínez JA, Pech-Canul MI, Hernández MB, Glot AB, Rodrígez E, Gracía-Ortiz L. Effect of Cr$_2$O$_3$ on the microstructure and non-ohmic properties of (Co, Sb)-doped SnO$_2$ varistor. Rev Mex Fis. 2013;59:6–9.

[66] Qi P, Wang JF, Su WB, Cheng HC, Zang GZ, Wang CM, Ming BQ. (Yb,Co,Nb)-doped SnO$_2$ varistors ceramics. Mater Sci Eng B. 2005;119:94–98. DOI: 10.1016/j.mseb.2004.11.013

[67] Wang WX, Wang JF, Chen HC, Su WB, Jiang B, Zang GZ, Wang CM, Qi P. Varistor properties of Sc$_2$O$_3$-doped Sn.Co.Nb ceramics. Ceram Int. 2005;31:287–291. DOI: 10.1016/j.ceramint.2004.05.018

[68] Leite DR, Las WC, Zaghete MA, Cilense M, Varela JA. The effect of Cr concentration and preparation method on the microstructure and electrical characterization of SnO$_2$-based ceramics. Mater Res. 2003;6:457–461. DOI: 10.1590/S1516-14392003000400005

[69] Aguilar-Martínez JA, Rodríguez E, García-Villarreal S, Falcon-Franco L, Hernandez. Effect of Ca, Sr and Ba on the structure, morphology and electrical properties of (Co,Sb)-doped SnO$_2$ varistors. Mater Chem Phys. 2015;153:180–186. DOI: 10.1016/j.matchemphys. 2015.01.001

[70] Qi P, Wang JF, Su WB, Chen HC, Zang GZ, Wang CM, Ming BQ. (Er, Co, Nb)-doped SnO$_2$ varistor ceramics. Mater Chem Phys. 2005;92:578–584. DOI: 10.1016/j.matchemphys.2005.02.013